



Received: 09/08/2024

Revised: 23/12/2024

Accepted: 18/03/2025

Published online: 31/03/2025

Research Article



Open Access under the CC BY -NC-ND 4.0 license

UDC 539.171.016

## ANALYSIS OF THE EFFECT OF THE B3Y-FETAL POTENTIAL ON ENERGY NEAR THE COULOMB BARRIER FOR THE ${}^9\text{Be}+{}^{12}\text{C}$ SYSTEM

Soldatkhan D., Baratova A.A.\*

L.N. Gumilyov Eurasian National University, Astana, Kazakhstan

\*Corresponding author: [aa.baratova@yandex.kz](mailto:aa.baratova@yandex.kz)

**Abstract.** The experimental data of the elastic scattering process of the  ${}^9\text{Be}+{}^{12}\text{C}$  nuclear system were analyzed from the point of view of microscopic theory in energy near the Coulomb barrier. The new Botswana 3-Yukawa -Fetal potential, created in a variational approach with lower-order constraints on two body matrices, was first used for the  ${}^9\text{Be}+{}^{12}\text{C}$  system as a real part of the optical potential. In the double folding model, density-dependent parameters were introduced into the nucleon density distribution formula, and they were applied to the Botswana 3-Yukawa - Fetal and Michigan 3-Yukawa - Paris potentials based on effective nucleon-nucleon interactions. As a result, modified real microfolding potentials were created. The results of a semi-microscopic analysis calculated on the basis of new microfolding potentials were presented. The uniqueness of the research lies in the calculation of density-dependent parameters based on the incompressibility coefficient, which characterizes the saturation properties of the nuclear medium. The equations of state of the elastic scattering process were formulated at the saturation density ( $\rho_0=0.17\text{ fm}^{-3}$ ), determined from the density dependence of the nuclear binding energy. The analysis results allow for a more accurate determination of nuclear properties and enhance the saturation properties of the nuclear medium. The efficiency of the new real potential was determined from a microscopic perspective, and the optimal parameters of the optical potential were found.

**Keywords:** microscopic analysis, elastic scattering, double folding model, B3Y-Fetal.

### 1. Introduction

Accurate determination of the depth of the potential of the interaction of a  ${}^9\text{Be}$  ion accelerated at low energy with light nuclei, the calculation of the contribution of the cluster transition mechanism is important in nuclear astrophysics. The study of the interaction of radioactive  ${}^9\text{Be}$  ion radiation with light nuclei in nuclear power plants is an urgent problem in the energy sector. In a reactor, the neutron source controlling the chain reaction is beryllium mixed with an alpha emitter. Alpha particles formed as a result of decay lead to the release of neutrons from beryllium when it turns into a  ${}^{12}\text{C}$  - core.

It is known from Rutherford's experience that the study of experimental data on elastic scattering at energies close to the Coulomb barrier is the main way to obtain information about the structure of the nucleus. Analysis of compound particle scattering in low-energy nuclei is an important source of information about the properties of the inter-nuclear potential [1]. The formation of the experimental cross-section in the process of elastic scattering was explained in the optical model by the fact that the real part of the optical potential (OP) depends on potential scattering, and the imaginary part as absorption depends on the mechanisms of cluster transition. In recent years, microscopically, the description of a real part of an op in the context of a form of local density based on effective nucleon-nucleon (NN) forces has given correct

results [2-5]. The Michigan 3-Yukawa (M3Y) potential of effective NN interactions can be improved based on the density-dependent form of nucleon distribution proposed by Dao T. Khoa [6-8]. The traditional M3Y-Reid, M3Y-Paris potentials defined in the tensor correlation calculation of Yukawa matrix elements have been in use for many years [7-9]. Recently, a new B3Y-Fetal potential was developed, calculated on the basis of a low-order limited variation approach [10]. This was a new step in the position of microscopic theory. Botswana 3-Yukawa (B3Y)-Fetal potential Ochala I., Fiase J.O. scientists have successfully used in symmetric  $^{16}\text{O}+^{12}\text{C}$ ,  $^{12}\text{C}+^{12}\text{C}$  systems and found that M3Y interaction is very similar in many channels [11-12]. In double folding model (DFM), a real part of the OP is created and density-dependent parameters are entered. In the overlapping region of the nucleons of the colliding nuclei, the central part of the effective NN interaction accumulates, which makes it possible to characterize the properties of the nucleus. The equations of state created in this central region depend on the density of the nucleus, the saturation property of the medium.

We conducted a comparative study in order to increase the saturation property of the medium by applying the potentials B3Y-Fetal, M3Y-Paris to the  $^9\text{Be}+^{12}\text{C}$  system. From this, the results of a semi-microscopic analysis of experimental data of elastic scattering at energies of  $E_{\text{lab}}=13$  MeV,  $E_{\text{lab}}=17.3$  MeV,  $E_{\text{lab}}=20$  MeV near the Coulomb barrier were presented. Modified folding potentials in the form of CDM3Y2-Paris and CDB3Y2-Fetal were tested. The results of the analysis are used in nuclear astrophysics in describing the initial nucleosynthesis and hydrostatic combustion of stars and as a way to know exactly the rate of nuclear reactions, to construct the nuclear state equations of a complex compound.

## 2. Calculation of the K - incompressibility factor depending on the saturation property of the nucleus

To increase the saturation property of nuclear matter, the equilibrium condition of the density-dependent specific bond energy is sufficient. To satisfy this saturation condition, calculated density – dependent parameters that depend on K - incompressibility must be introduced into the effective M3Y interaction. In particular, it is necessary to construct equations of state at value  $\rho_0=0,17$   $\text{fm}^{-3}$  of the saturation density of nuclear matter.

Specific binding energy of density-dependent infinite nuclear matter [13]:

$$\frac{\varepsilon_0}{A}(\rho) = \frac{3\hbar^2 k_F^2}{10m} + F(\rho) \frac{\rho}{2} (J_D + \int [\bar{j}_1(k_F r)]^2 v^{EX}(r) d^3r) \quad (1)$$

where m - is the nucleon mass,  $J_D$ - volume integral,  $\bar{j}_1(x)$  - Bessel spherical function,  $\rho$  - nucleon density,  $k_F$  - Fermi pulse.

From the equilibrium saturation condition of the binding energy of the nucleus [13]:

$$\frac{d\varepsilon}{d\rho} = \frac{\hbar^2 k_F^2}{5mp} + \frac{J_D C}{2} \left(1 - \frac{5}{3} \beta(\varepsilon) \rho^{\frac{2}{3}}\right) = 0 \quad (2)$$

From equation (2), the formula for bond energy, which depends on the density parameters, is written as follows:

$$\varepsilon = \frac{3\hbar^2 k_F^2}{10m} + \frac{\rho J_D}{2} C \left(1 - \beta(\varepsilon) \rho^{\frac{2}{3}}\right) \quad (3)$$

Density-dependent parameters and saturation density [13]:

$$C = - \frac{2\hbar^2 k_F^2}{5m J_D \rho \left(1 - \frac{5}{3} \beta(\varepsilon) \rho^{\frac{2}{3}}\right)} \quad (4)$$

$$\beta(\varepsilon) = \frac{(3-3p)}{(9-5p)} \cdot \frac{1}{\rho^{5/3}} \quad (5)$$

$$\rho_0 = -\frac{10m\varepsilon}{\hbar^2(1.5\pi^2\rho)^{2/3}} \quad (6)$$

The nuclear incompressibility factor is calculated by the following equation [13]:

$$K_\alpha = -\left[\frac{3\hbar^2 k_F^3}{5m} + 5J_D C\beta(\varepsilon)\rho^{5/3}\right]_{\rho=\rho_0} \quad (7)$$

The following figure shows a curve of dependence of the specific binding energy of the nucleus on the density of nucleons. The saturation density point corresponds to the value  $\rho_0=0,17 \text{ fm}^{-3}$ .

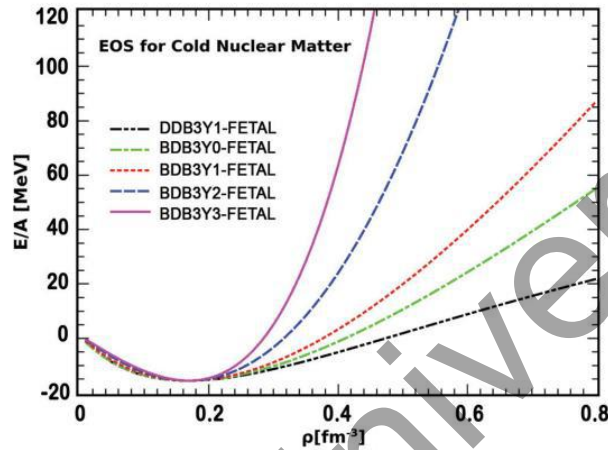


Fig.1. Saturation point of the density dependence of the binding energy of the nucleus [14]

### 3. Interaction on effective NN forces M3Y-Paris and B3Y-Fetal potentials

The interaction of M3Y is the sum of the  $U^D(\vec{R})$  - direct and  $U^{EX}(\vec{R})$  - exchange potentials by effective NN forces.

$$U(\vec{R}) = U^D(\vec{R}) + U^{EX}(\vec{R}) \quad (8)$$

Direct potential [15, 16]:

$$U^D(\vec{R}) = \iint \rho^{(1)}(\vec{r}_1) v_D(\vec{s}) \rho^{(2)}(\vec{r}_2) d\vec{r}_1 d\vec{r}_2 \quad (9)$$

where  $v_D(\vec{s})$  - direct component of effective interaction,  $\rho^{(1)}(\vec{r}_1)$ ,  $\rho^{(2)}(\vec{r}_2)$  - nucleon density of colliding nuclei,  $s = r_2 - r_1 + R$

Exchange potential [16, 17]:

$$U^{EX}(\vec{R}) = \iint \rho^{(1)}(\vec{r}_1, \vec{r}_1 + \vec{s}) v_{EX}(\vec{s}) \rho^{(2)}(\vec{r}_2, \vec{r}_2 - \vec{s}) \exp[i\vec{k}(\vec{R})\vec{s}/\eta] d\vec{r}_1 d\vec{r}_2 \quad (10)$$

where  $v_{EX}(\vec{s})$  - effective NN interaction exchange component,  $\rho^{(1)}(\vec{r}_1, \vec{r}_1 + \vec{s})$ ,  $\rho^{(2)}(\vec{r}_2, \vec{r}_2 - \vec{s})$  - density matrix of colliding nuclei.

For the calculation of potentials, it is important to clearly take into account the transition effects of NN - interaction [13]:

$$v_{D(EX)} = 1/16 (3v_{TE}^c + 3v_{SE}^c \pm 9v_{T0}^c \pm v_{S0}^c) \quad (11)$$

where  $(v_{TE}^c, v_{SE}^c)$ ,  $(v_{T0}^c, v_{S0}^c)$  - triplet and singlet components of central forces.

Direct and exchange components based on the G-matrix element of the M3Y-Paris potential [18]:

$$v_D(s) = 11061,6 \frac{\exp(-4s)}{4s} - 2537,5 \frac{\exp(-2,5s)}{2,5s} \quad (12)$$

$$v_D(s) = -1524,0 \frac{\exp(-4s)}{4s} - 518,8 \frac{\exp(-2,5s)}{2,5s} - 7,8474 \frac{\exp(-0,7072s)}{0,7072s} \quad (13)$$

B3Y-Fetal radial form of the isoscalar portion of interaction [10]:

$$v_D(s) = 10472,13 \frac{\exp(-4s)}{4s} - 2203,11 \frac{\exp(-2,5s)}{2,5s} \quad (14)$$

$$v_{EX}(s) = 499,63 \frac{\exp(-4s)}{4s} - 1347,77 \frac{\exp(-2,5s)}{2,5s} - 7,8474 \frac{\exp(-0,7072s)}{0,7072s} \quad (15)$$

#### 4. The theoretical basis of semi-microscopic analysis

When analyzing experimental data of elastic scattering within the framework of an optical model (OM), the Woods-Saxon form of potential was used.

$$U(r) = V_o \left[ 1 + \exp\left(\frac{r-R_V}{a_V}\right) \right] - iW_o \left[ 1 + \exp\left(\frac{r-R_W}{a_W}\right) \right] + V_C(r) \quad (16)$$

where  $V_o$ ,  $W_o$ ,  $a_V$ ,  $a_W$ ,  $R_V$ ,  $R_W$  are real, imaginary potentials, diffusion, radius,  $V_C(r)$  is the Coulomb potential.

In a semi-microscopic analysis, the optical potential of the interacting nuclei is calculated by the following formula [7]:

$$U(r) = N_r [v_D(s) + v_{EX}(s)] - iW_o f(r, r_w, a_w) + V_C(r) \quad (17)$$

where  $v_D(s)$ ,  $v_{EX}(s)$  – direct and exchange components of interaction potential,  $N_r$  – renormalization factor.  $W_o$ ,  $r_w$ ,  $a_w$  – imaginary potential, radius, diffusion,  $V_C(r)$  – Coulomb potential.

The direct and exchange components of the real potential are calculated on the basis of DFM, resulting in the folding potential.

$$v_D(s) + v_{EX}(s) = V_F(r) \quad (18)$$

For the imaginary part of the optical potential, we use the woods-Saxon form factor in volumetric form.

$$U(r) = N_r V_F(r) - iW_o \left[ 1 + \exp\left(\frac{r-r_w}{a_w}\right) \right] + V_C(r) \quad (19)$$

$V_C(r)$  - Coulomb potential [16],

$$V_C(R) = \begin{cases} \frac{Z_1 Z_2 e^2}{2R_C} \left( 3 - \frac{R^2}{R_C} \right) & \text{For } R \leq R_C \\ \frac{Z_1 Z_2 e^2}{R} & \text{For } R \geq R_C \end{cases} \quad (20)$$

M3Y-Paris and B3Y-Fetal potentials are density and energy dependent.

$$v_{D(EX)}(E, \rho, s) = F(E, \rho) g(E) v_{D(EX)}(s), \quad (21)$$

A formfactor proposed based on the density-dependent parameters [19]

$$F(\rho) = C[1 + \alpha \exp(-\beta\rho) - \gamma\rho^n] \quad (22)$$

the energy-dependent factor  $g(E)$  is expressed as [7]:

$$g(E) = 1 - 0.003(E/A) \quad (23)$$

The nuclear matter density distribution was calculated in the harmonic-oscillator model [20, 2]:

$$\rho(r) = \rho_0(1 + \alpha(r/a)^2) \exp(-(r/a)^2) \quad (24)$$

where  $\rho_0=0,17 \text{ fm}^{-3}$ ,  $\alpha$  (alfa) and  $a$  are charge density distribution parameters. For the  ${}^9\text{Be}$  core,  $\alpha=1.77 \text{ fm}$ ,  $a=0.631 \text{ fm}$ , and for the  ${}^{12}\text{C}$  core,  $\alpha=1.687 \text{ fm}$ ,  $a=1.067 \text{ fm}$  [20].

**Table 1.** Density-dependent parameters [8, 14].

| Density dependence           | $C$    | $a$    | $\beta \text{ (fm}^3\text{)}$ | $\gamma \text{ (fm}^3\text{)}$ | $K \text{ (MeV)}$ |
|------------------------------|--------|--------|-------------------------------|--------------------------------|-------------------|
| CDM3Y2-Paris<br>CDB3Y2-Fetal | 0.3346 | 3.0357 | 3.0685                        | 1.0                            | 204               |
| CDB3Y3-Fetal                 | 0.2985 | 3.4528 | 2.6388                        | 1.5                            | 217               |

## 5. Discussion of results

At energies of  $E_{\text{lab}}=13.0 \text{ MeV}$ ,  $E_{\text{lab}}=17.3 \text{ MeV}$ ,  $E_{\text{lab}}=20.0 \text{ MeV}$  near the Coulomb barrier for the  ${}^9\text{Be}+{}^{12}\text{C}$  system, the density-dependent CDM3Y2-Paris, CDB3Y2-Fetal and CDB3Y3-Fetal folding potentials were built on the basis of the DFM model. From the picture, the depth of the CDB3Y2-Fetal and CDB3Y3-Fetal potentials was more sensitive than that of the CDM3Y2-Paris version. Theoretical calculations of semi-microscopic analysis were performed on the basis of the FRESKO code [21]. The following figure shows the results of a semi-microscopic analysis of experimental sections of elastic scattering for the  ${}^9\text{Be}+{}^{12}\text{C}$  system.

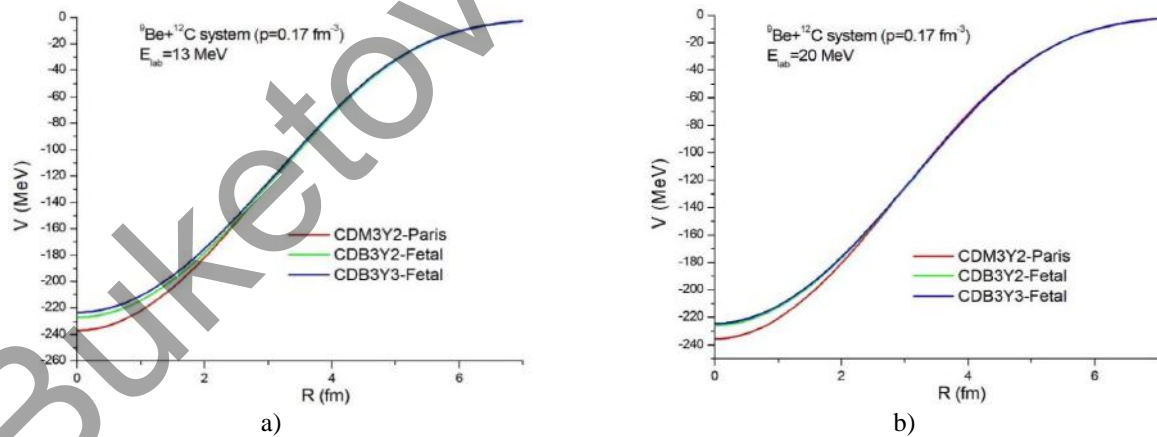


**Fig.2.** The depth of the generated real DF potentials for the  ${}^9\text{Be}+{}^{12}\text{C}$  system at:  
a)  $E_{\text{lab}} = 13.0 \text{ MeV}$  and b)  $E_{\text{lab}} = 20.0 \text{ MeV}$  energies

Theoretical cross-sections at an energy of  $E_{\text{Lab}}=13 \text{ MeV}$  described the experimental cross-section in the range of up to  $90^\circ$ , as can be seen from the images. This is because at low energies close to the Coulomb barrier, the scattering process prevails over the absorption process. Therefore, the share of the imaginary potential is small. And to characterize the increase in the Section at large angles after  $90^\circ$ , it is necessary to take into account the proportion of the cluster transition. The following figures show the dependence of the normalized scattering cross-section ( $d\sigma/d\sigma_{\text{Ruth}}$ ) on the scattering angle ( $\theta_{\text{cm}}$ ) in the center-of-mass system for the  ${}^9\text{Be}+{}^{12}\text{C}$  nuclear system at incident energies of  $E_{\text{Lab}}=13.0 \text{ MeV}$ ,  $E_{\text{Lab}}=17.3 \text{ MeV}$ , and  $E_{\text{Lab}}=20.0 \text{ MeV}$ .

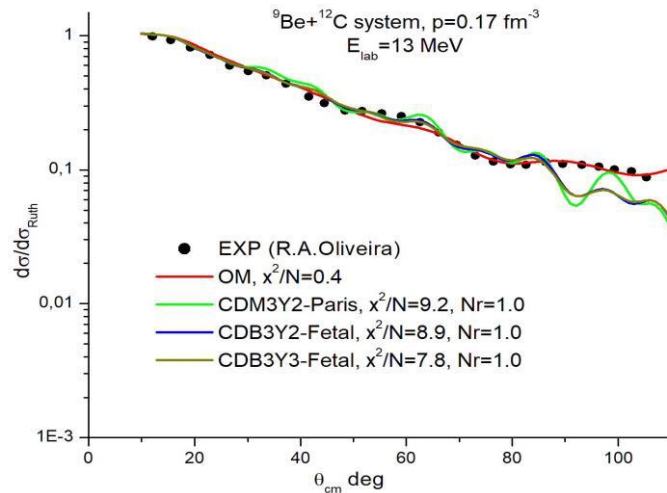


Fig.3. The result of the analysis at energy  $E_{\text{Lab}}=13 \text{ MeV}$

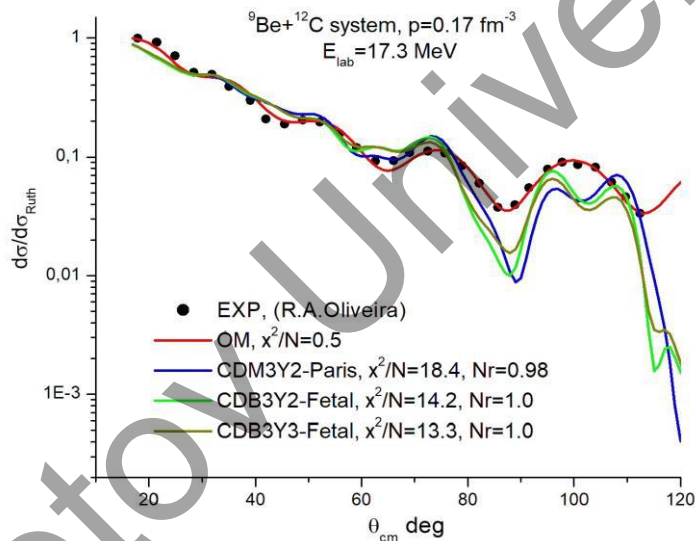


Fig.4. The result of the analysis at energy  $E_{\text{Lab}}=17.3 \text{ MeV}$

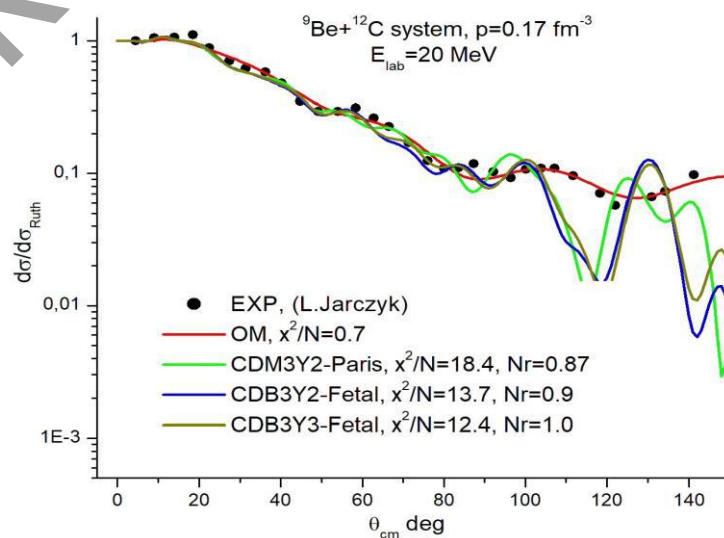


Fig.5. The result of the analysis at energy  $E_{\text{Lab}}=20 \text{ MeV}$

The optical model (OM) potential parameters presented in Table 2 were calculated using equation (16), while the semi-microscopic model (DFOM) parameters were calculated using equation (17). The calculations were performed based on the FRESKO code.

**Table 2.** The values of the optimal parameters of the elastic scattering Section at energies  $E_{\text{Lab}}=13.0$  MeV,  $E_{\text{Lab}}=17.3$  MeV,  $E_{\text{Lab}}=20.0$  MeV for the  ${}^9\text{Be}+{}^{12}\text{C}$  system are shown in the following table.

| E, MeV | Model | WS parameters and types of DF potential |            |            | $N_r$ | Parameters of the imaginary potential WS |            |            | $\sigma_R$ , mb | $\chi^2/N$ |
|--------|-------|---|------------|------------|-------|--|------------|------------|-----------------|------------|
|        |       | $V_0$ , MeV                             | $r_V$ , fm | $a_V$ , fm |       | $W_0$ , MeV                              | $r_W$ , fm | $a_W$ , fm |                 |            |
| 13.0   | OM    | 65.8                                    | 1.69       | 0.12       | -     | 5.36                                     | 1.74       | 1.19       | 2211            | 0.4        |
|        | DFOM  | CDM3Y2-Paris                            |            |            | 1.0   | 5.36                                     | 1.88       | 0.9        | 2037            | 9.25       |
|        | DFOM  | CDB3Y2-Fetal                            |            |            | 1.0   | 5.36                                     | 1.88       | 0.9        | 2134            | 8.9        |
|        | DFOM  | CDB3Y3-Fetal                            |            |            | 1.0   | 5.36                                     | 1.88       | 0.9        | 2129            | 7.8        |
| 17.3   | OM    | 28.5                                    | 1.28       | 0.62       | -     | 5.6                                      | 1.49       | 0.19       | 1088            | 0.5        |
|        | DFOM  | CDM3Y2-Paris                            |            |            | 0.98  | 5.5                                      | 1.45       | 0.9        | 1508            | 18.4       |
|        | DFOM  | CDB3Y2-Fetal                            |            |            | 1.0   | 5.5                                      | 1.45       | 0.9        | 1492            | 14.2       |
|        | DFOM  | CDB3Y3-Fetal                            |            |            | 1.0   | 5.5                                      | 1.45       | 0.9        | 1501            | 13.3       |
| 20.0   | OM    | 154.7                                   | 1.06       | 0.17       | -     | 10.6                                     | 0.78       | 1.48       | 1352            | 0.7        |
|        | DF    | CDM3Y2-Paris                            |            |            | 0.87  | 6.59                                     | 1.44       | 0.63       | 1151            | 19.8       |
|        | DF    | CDB3Y2-Fetal                            |            |            | 0.9   | 6.59                                     | 1.44       | 0.63       | 1163            | 19.8       |
|        | DF    | CDB3Y2-Fetal                            |            |            | 1.0   | 6.59                                     | 1.44       | 0.63       | 1158            | 19.8       |

The  $N_r$  - factor of semi-microscopic analysis was determined close to 1.0. From this you can see the good result of the new CDB3Y2-Fetal, CDB3Y3-Fetal folding potentials, which is created as a real potential. As a relative error of experimental and theoretical sections, the values of the  $\chi^2/N$  - parameter did not exceed 20 percent. Weak values of  $W_0$  - imaginary potential 1 indicate the opacity of the optical potential to be determined for system  ${}^9\text{Be}+{}^{12}\text{C}$ . The fact that the values of the  $W_0$ ,  $r_W$ ,  $a_W$  - Woods-Saxon parameters are unchanged in different models again proves the truthfulness of the real potential. The dependence of the  $\sigma_R$  - cross section on the beam energy is preserved in all models (OM, DFOM). The CDB3Y2-Fetal, CDB3Y3-Fetal folding potentials created at an energy close to the Coulomb barrier were investigated relative to the CDM3Y2-Paris variant.

## 6. Conclusion

For the  ${}^9\text{Be}+{}^{12}\text{C}$  system, a new B3Y-Fetal potential based on variational calculations was used for the first time in a semi-microscopic analysis. Studying the effectiveness of the new B3Y-Fetal potential was important from the point of view of applying the theoretical breakthrough. At the energy close to the Coulomb barrier, the real part of the optical potential shows dominance in the mechanism of elastic scattering cross-section formation. The CDM3Y2-Paris, CDB3Y2-Fetal and CDB3Y3-Fetal folding potentials were established, elastic scattering sections and optimal parameters were determined. Were able to describe the experimental data on the basis of K - incompressibility dependent parameters calculated for the actual density of  $\rho_0=0.17$  fm<sup>-3</sup> - in accordance with the saturation condition of nuclear matter. So we were able to increase the saturation property of the nuclear medium.

The result of the work makes it possible to determine the interaction characteristics of heavy ions up to a very small inter-core distance. The results obtained are used in nuclear astrophysics for model calculations of nuclear reactions.

**Conflict of interest statement**

The authors declare that they have no conflict of interest in relation to this research, whether financial, personal, authorship or otherwise, that could affect the research and its results presented in this paper.

**CRedit author statement.**

**Soldatkhan, D.** - performed theoretical calculations and analysis; **Baratova, A.A.** - supervised the work carried out in the research. The final manuscript was read and approved by all authors.

**Acknowledgments**

We thank the participants who made this research possible.

**References**

- 1 Soldatkhan D., Amangeldi N., Baltabekov A., Yergaliuly G. (2022) Investigation of the energy dependence of the interaction potentials of the  $^{16}\text{O}+^{12}\text{C}$  nuclear system with a semi-microscopic method. *Eurasian Physical Technical Journal*, 19, 3(41), 39 – 44. <https://doi.org/10.31489/2022No3/39-44>
- 2 Masadeh S.B., Abdallah D.A., Jaghoub M.I. (2023) Analysis of nucleon-nucleus scattering data using a density-dependent semi-microscopic optical model with channel coupling. *Physical Review C*, 107(2) 024616. <https://doi.org/10.1103/PhysRevC.107.024616>
- 3 Morzabayev A., Amangeldi N., Awad A. Ibraheem, Soldatkhan D., Yergaliuly G., Mauey B., Anuar A. O., Hamada. Sh. (2023) Dynamics of  $^7\text{Li}$  Breakup and its Influence on Elastic Scattering: A Study of  $^7\text{Li}+^{144}\text{Sm}$  System. *Chinese Physics C*, 4, 31 - 40. <https://doi.org/10.1055/s12138-135-01108-0>
- 4 Soldatkhan D., Amangeldi N., Makhanov K.M., Smagulov Zh.K. (2023) Application of the new B3Y-Fetal potential in the semi-microscopic analysis of the scattering of accelerated  $^6\text{Li}$  - lithium and  $^{16}\text{O}$  - oxygen nuclei from the  $^{12}\text{C}$  - carbon nucleus. *Eurasian Physical Technical Journal*, 25, 4(46), 22 - 30. <https://doi.org/10.31489/2023No4/17-22>
- 5 Mauey B., Amangeldi N., Raiymbekov Y., Soldatkhan D., Al-Jahwashi E., Awad A. Ibraheem, Al-Ghamdi A.H., Hamada Sh. (2024) Deuteron breakup effects on the  $d+^{12}\text{C}$ ,  $^{15}\text{N}$ ,  $^{16}\text{O}$ ,  $^{24}\text{Mg}$ ,  $^{32}\text{S}$ ,  $^{58}\text{Ni}$ , and  $^{70}\text{Ge}$  elastic scattering angular distributions. *Chinese Journal of Physics*, 90, 155-165. <https://doi.org/10.1016/j.cjph.2024.05.003>
- 6 Amangeldi N., Burtebayev N., Soldatkhan D., Maulen Nassurlla, Mauey B., Yergaliuly G., Marzhan Nassurlla, Awad A. Ibraheem, Hamada, Sh. (2024) Recent Measurement and Theoretical Analysis for the Elastic Scattering of the  $15\text{N}+^{11}\text{B}$  System. *Brazilian Journal of Physics*, 54(5), 169. <https://doi.org/10.1007/s13538-024-01547-2>
- 7 Khoa D.T., Phuc N. H., Loan D. T., Loc B.M. (2016) Nuclear mean field and double-folding model of the nucleus-nucleus optical potential. *Physical Review C*, 94(3), 034612. <https://doi.org/10.1103/PhysRevC.94.034612>
- 8 Khoa D.T., Satchler G.R., Von Oertzen W. (1997) Nuclear incompressibility and density dependent NN interactions in the folding model for nucleus-nucleus potentials. *Physical Review C*, 56(2), 954. <https://doi.org/10.1103/PhysRevC.56.954>
- 9 Amangeldi N., Burtebayev N., Artemov S.V., Maulen Nassurlla, Mauey B., Yergaliuly G., Marzhan Nassurlla, Ergashev F.Kh., Soldatkhan D., Shaudirbayeva D.S., Awad A., Ibraheem, Hamada Sh. (2024) Efficiency of the new B3Y-fetal potential in the analysis of the elastic and inelastic angular distributions for the  $10\text{B}+^{12}\text{C}$  system. *Pramana*, 98(3), 106. <https://doi.org/10.1007/s12043-024-02760-z>
- 10 Fiase J.O., Devan K.R.S., Hosaka A. (2002) Mass dependence of M3Y-type interactions and the effects of tensor correlations. *Physical Review C*, 66(1), 014004. <https://doi.org/10.1103/PhysRevC.66.014004>
- 11 Ochala I., Fiase J.O. Gbaorun F., Bamikole J.A. (2021) A study of asymmetric nuclear matter with the B3Y-Fetal effective interaction. *International Research Journal of Pure and Applied Physics*, 8(2), 10 - 35. <https://doi.org/10.37745/irjppap.13>
- 12 Ochala I., Fiase J.O. (2021) B3Y-Fetal effective interaction in the folding analysis of elastic scattering of  $^{16}\text{O}+^{16}\text{O}$ . *Nuclear Science and Techniques*, 32(8), 81. <https://doi.org/10.1007/s41365-021-00920-z>
- 13 Ochala J. O. Fiase E. Anthony. (2017) Computation of nuclear binding energy and incompressibility with a new M3Y - type effective interaction. *International Research Journal of Pure and Applied Physics*, 5(3), 5 - 13.
- 14 Ochala I., Fiase J.O. (2018) Symmetric nuclear matter calculations: A variational approach. *Physical Review C*, 98(6), 064001. <https://doi.org/10.1103/PhysRevC.98.064001>
- 15 Khoa N.H.D., Tan N. H., Khoa D. T. (2022) Spin symmetry energy and equation of state of spin-polarized neutron star matter. *Physical Review C*, 105(6), 065802. <https://doi.org/10.1103/PhysRevC.105.065802>
- 16 Hassanain M.A., Alqahtani F.M., Ibraheem A.A., Anwar M., Behary K.O., Mahmoud Z.M., El-Azab Farid M. (2018) Elastic and inelastic  $\text{O}^{16}+\text{C}^{12}$  rainbow scattering within the coupled-channels mechanism. *Physical Review C*, 98(1), 014621. <https://doi.org/10.1103/PhysRevC.98.014621>

- 17 Morzabayev A., Amangeldi N., Awad A. Ibraheem, Yergaliuly G., Mauey B., Hamada Sh. (2024) Detailed analysis of the  ${}^6\text{Li}$  breakup in the field of the  ${}^{209}\text{Bi}$  nucleus. *Physica Scripta*, 99. 025307. <https://doi.org/10.1088/1402-4896/ad1d43>
- 18 Khoa D. T., Loan D. T., Phuc N. H. (2024) Pauli nonlocality and the nucleon effective mass. *Physical Review C*, 110(2), 024607. <https://doi.org/10.1103/PhysRevC.110.024607>
- 19 Khoa D.T., Von Oertzen W., Bohlen H.G., Ohkubo S. (2007) Nuclear rainbow scattering and nucleus–nucleus potential. *Journal of Physics G: Nuclear and Particle Physics*, 34(3), R111. <https://doi.org/10.1088/0954-3899/34/3/R01>
- 20 De Vries H., De Jager C.W., De Vries C. (1987) Nuclear charge-density-distribution parameters from elastic electron scattering. *Atomic data and nuclear data tables*, 36(3), 495-536. [https://doi.org/10.1016/0092-640X\(87\)90013-1](https://doi.org/10.1016/0092-640X(87)90013-1)
- 21 Thompson I.J. (1988) Getting started with FRESKO. *Comput. Phys. Rep*, 7, 167-212. [https://doi.org/10.1016/0167-7977\(88\)90005-6](https://doi.org/10.1016/0167-7977(88)90005-6)

---

#### AUTHORS' INFORMATION

**Soldatkhan, D.** - PhD, Senior Lecture, Department of Radio Engineering, Electronics and Telecommunications, L.N. Gumilyov Eurasian National University, Astana, Kazakhstan; Scopus Author ID: 57768566200; <https://orcid.org/0000-0001-7981-4100>; [Soldathan.dauren@mail.ru](mailto:Soldathan.dauren@mail.ru)

**Baratova, A.A.** – Candidate of Physical and Mathematical Sciences, Senior Lecturer, Department of Nuclear Physics, New Materials and Technologies, L.N. Gumilyov Eurasian National University, Astana, Kazakhstan; Scopus Author ID: 57217354220, <https://orcid.org/0000-0002-1263-0734>; [aa.baratova@yandex.kz](mailto:aa.baratova@yandex.kz)